DNA Interaction, Antimicrobial, Anticancer Activities and Molecular Docking Study of Some New VO(II), Cr (III), Mn(II) and Ni(II) Mononuclear Chelates encompassing Quaridentate imi…

Article *in* Journal of Photochemistry and Photobiology B Biology · April 2017

DOI: 10.1016/j.jphotobiol.2017.04.003

CITATIONS
6

READS
1,721

4 authors:

Laila H. Abdel-Rahman
Sohag University
82 PUBLICATIONS **698** CITATIONS
SEE PROFILE

Ahmed M. Abudief
Sohag University
93 PUBLICATIONS **682** CITATIONS
SEE PROFILE

Moustafa O. Aboelez
Sohag University
8 PUBLICATIONS **9** CITATIONS
SEE PROFILE

Azza Hassan
Sohag University
8 PUBLICATIONS **14** CITATIONS
SEE PROFILE

Journal of Photochemistry & Photobiology, B: Biology 170 (2017) 271–285

Contents lists available at ScienceDirect

Journal of Photochemistry & Photobiology, B: Biology

journal homepage: www.elsevier.com/locate/jphotobiol

DNA interaction, antimicrobial, anticancer activities and molecular docking study of some new VO(II), Cr(III), Mn(II) and Ni(II) mononuclear chelates encompassing quaridentate imine ligand

Laila H. Abdel-Rahman[a], Ahmed M. Abu-Dief[a,*], Moustafa O. Aboelez[b], Azza A. Hassan Abdel-Mawgoud[a]

[a] Chemistry Department, Faculty of Science, Sohag University, 82524, Egypt
[b] Department of Pharmaceutical Chemistry, Faculty of Pharmacy, Sohag University, Egypt

ARTICLE INFO

Keywords:
Imines
Chelates
Thermal analyses
Antimicrobial activity
DNA interaction
Anticancer
Molecular docking analysis

ABSTRACT

The present study was conducted to synthesis of some new imine Cr(III), VO(II), Mn(II) and Ni(II) complexes derived from the condensation of 2-amino phenol with 2-hydroxynapthaldehyde were synthesized. The prepared HNPN imine ligand was analyzed by its melting point, IR, ^{1}H NMR and ^{13}C NMR spectroscopies. The investigated HNPN imine complexes were characterized by elemental analysis, FT IR, UV–vis and thermal analysis (TGA) under nitrogen atmosphere from ambient temperature to 750 °C. The experimental results revealed that the investigated complexes contain hydrated water molecules. The molar conductance values of complexes are relatively low, indicating the non-electrolytic nature of these complexes. Magnetic susceptibility measurements show that the investigated complexes are paramagnetic. Moreover, the stability constants of the preparing complexes were determined spectrophotometrically. All the complexes were found to be monomeric 1:1 (M:L) stoichiometry in nature with octahedral geometry for Cr(III), tetrahedral for Mn(II), square planner for Ni(II) and square pyramidal for VO(II). Moreover, the prepared HNPN imine ligand and its complexes were evaluated for antimicrobial effect against some types of bacteria such as *Bacillus subtilis (+ ve)*, *Escherichia coli (− ve)* and *Staphylococcus aureus (+ ve)* and some types of fungi such as *Aspergillus niger*, *Candida glabrata* and *Trichophyton rubrum*. The results of these studies indicate that the metal complexes exhibit a stronger antibacterial and antifungal efficiency compared to their corresponding imine ligand. Moreover, the interaction of the investigated complexes with CT-DNA was checked using spectral studies, viscosity measurements and gel electrophoreses. The absorption titration studies revealed that each of these complexes is an avid binder to calf thymus-DNA. Also, there was appreciable changes in the relative viscosity of DNA, which is consistent with enhanced hydrophobic interaction of the aromatic rings and intercalation mode of binding. In addition to, the cytotoxic activity of the prepared imine complexes on human colon carcinoma cells, (HCT-116 cell line), hepatic cellular carcinoma cells, (HepG-2 cell line) and breast carcinoma cells (MCF-7 cell line) has cytotoxicity effect against growth of carcinoma cells compared to the clinically used Vinblastine standard. Furthermore, the molecular docking into TRK (PDB: 1t46) was done for the optimization of the investigated compounds as potential TRK inhibitors.

1. Introduction

Imines are an important class of inorganic and organic compounds with a variety of uses. They have been widely engaged as ligands in the formation of transition metal complexes [1,2]. Imines possess more interesting properties due to their diverse anticancer, antiviral, fungicidal, bactericidal, anti-inflammatory and anti-HIV activities [3–5]. Thus, the development of new chemotherapeutic imines is now attracting the attention of medicinal chemists [6]. The chemistry of Schiff base compounds as well as their metal complexes is of great interest in various fields of chemical and biological. Schiff base ligands are able to coordinate many different metals and to stabilize them in various oxidation states [7–10]. Small molecules can interact with DNA via the following three non -covalent modes: intercalation, groove binding and external electrostatic effects. Among these interactions, intercalation is one of the most important DNA binding modes, which is

* Corresponding author.
E-mail addresses: ahmed_benzoic@yahho.com, ahmedabudief@science.sohag.edu.eg (A.M. Abu-Dief).

http://dx.doi.org/10.1016/j.jphotobiol.2017.04.003
Received 30 January 2017; Received in revised form 11 March 2017; Accepted 6 April 2017
Available online 09 April 2017
1011-1344/

related to the antitumor activity of a compound [11–16]. Recently, there has been a great interest in the binding of metal complexes with DNA [17–23] because it may give important information for new cancer therapeutic agents and potential probes of DNA structure and conformation. Hence, much attention has been targeted on the design of metal based complexes, particularly transition metal complexes which can bind to and cleave DNA effectively. It is our aim to design an appropriate ligand to obtain the optimum metal complex to resolve the challenges that have arisen earlier. Thus, encouraged by the advancements discussed above, herein we report our newly HNPN imine ligand. The structure of the titled imine ligand was studied by ^{1}H NMR, ^{13}C NMR, IR, UV–Vis. Then it's, Cr(III), VO(II), Mn(II) and Ni(II) complexes were prepared and the spectral and thermal properties of these complexes were studied in details. Also the kinetic parameters for degradation steps in thermograms of these complexes were calculated. Indeed, the biological activity of the prepared HNPN imine ligand and its complexes was screened against selected kinds of bacteria and fungi. Moreover, the interaction of the complexes with CT-DNA was studied. Furthermore, the cytotoxic activity of the prepared imine complexes were tested against different cell lines and confirmed by docking studies.

2. Experimental

2.1. Material and Methods

All of the chemicals and solvents used for synthesis were of commercially available reagent grade and used without purification. They included 2-hydroxynapthaldehyde, 2-amino phenol, vanadyl acetylacetonate ($VO(C_5H_7O_2)_2$), Chromium nitrate ($Cr(NO_3)_3{\cdot}6H_2O$). and Nickel nitrate ($Ni(NO_3)_2{\cdot}6H_2O$) and $MnCl_2{\cdot}4H_2O$ were obtained from Sigma-Aldrich. Spectroscopic grade ethanol, dimethylformamide (DMF)and HCl products were used.

Melting point for the prepared imine ligand and decomposition temperatures for its prepared complexes were carried out on a melting point device, Gallenkamp, UK. Infrared spectra were recorded as KBr pellets using Shimadzu. FTIR-8300 spectrophotometer. Proton NMR spectra of the titled imine ligand and its HNPNNi complex were recorded with a Bruker Avance DPX-500 spectrometer. All of the scanning UV–Vis spectra in DMF were registered using 10 mm matched quartz cells through PG spectrophotometer model T + 80 in the wavelength range 200–800 nm. Elemental analyses which were made at main lab of Cairo University by Elemental analyzer Perkin-Elmer (model240c). The instrument employed for recording magnetic susceptibility were performed on Gouy's balance and the diamagnetic corrections were executed by Pascal's constants. Thermo gravimetric test was made under nitrogen with a heating rate 10 °C min^{-1} on Shimadzu corporation 60H analyzer. The absorbance values of 3×10^{-3} M of each complex were measured at various pH levels. The pH levels were checked by using a series of Britton universal buffers [11]. A HANNA 211 pH meter at 298 K equipped with a CL-51B combined electrode was used for pH measurements, calibrated against standard buffers (pH 4.02 and 9.18) before measurements.

2.2. Preparation of HNPN Imine Ligand

The tetra-dentate HNPN imine ligand (cf. Scheme 1) was synthesized by the condensation of ethanolic solution of 2-hydroxy-1-napthaldehyde (10 mmol, 1.72 g) with o-phenylenediamine (5 mmol, 0.54 g). The resulting reaction mixture was refluxed for 1 h at 80 °C. After that, solution was gradually evaporated to quarter of its original volume and then left to cool. The completion of the reaction mixture was monitored by TLC. The obtained orange and yellow crystals HNPN imine ligand was filtered. Then washed with cold ethanol several times and dried under reduced pressure in a desiccator ^{1}HNMR (δ, ppm), in DMSO: δ = 7.07 (d, ^{3}J = 7.8 Hz, 2H, H-3,3′), 7.38 (t, ^{3}J = 6.8 Hz, 2H, H-6,6′), 7.45 (s, 2H, H-10,13), 7.55 (t, ^{3}J = 7.1 Hz, 2H, H-11,12), 7.82 (dd, ^{3}J = 7.0 Hz, 4H, H-7,7′ and H-8,8′), 7.96 (d, ^{3}J = 7.5 Hz, 2H, H-5,5′), 8.53 (d, ^{3}J = 8.0 Hz, 2H, H-4,4′), 9.69 (s, 2H, CH═N), 15.02 ppm (s, 2H, –OH) (cf. Fig. S1).

^{13}CNMR (δ, ppm), in DMSO: δ = 109.8 (C_q), 120.2 (CH), 121.0 (CH), 121.8 (CH), 124.0 (CH), 127.4 (C_q), 127.7 (CH), 128.5 (CH), 129.4 (CH), 133.5 (C_q), 137.1 (CH), 139.2 (C_q), 158.0 (C_q), 168.7 ppm (CH═N) (cf. Fig. S2).

2.3. Synthesis of Complexes With HNPN as Quaridentate Imine Ligand

Cr(III), VO(II), Mn(II) and Ni(II) complexes were synthesized by the addition of 10 mmol of $Cr(NO_3)_3{\cdot}6H_2O$ (4.002 g); $VO(acac)_2$ (2.65 g); $MnCl_2{\cdot}4H_2O$ (1.98 g) or $Ni(NO_3)_2{\cdot}6H_2O$ (2.91 g) dissolved in 30 ml of ethanolic solution to a hot ethanolic solution 30 ml (10 mmol) of HNPN (4.17 g) imine ligand in molar ratio (1:1). The color of the resulted compound changed immediately. The resulting mixture was refluxed with stirring for 1 h. After evaporation the solvent, the precipitated

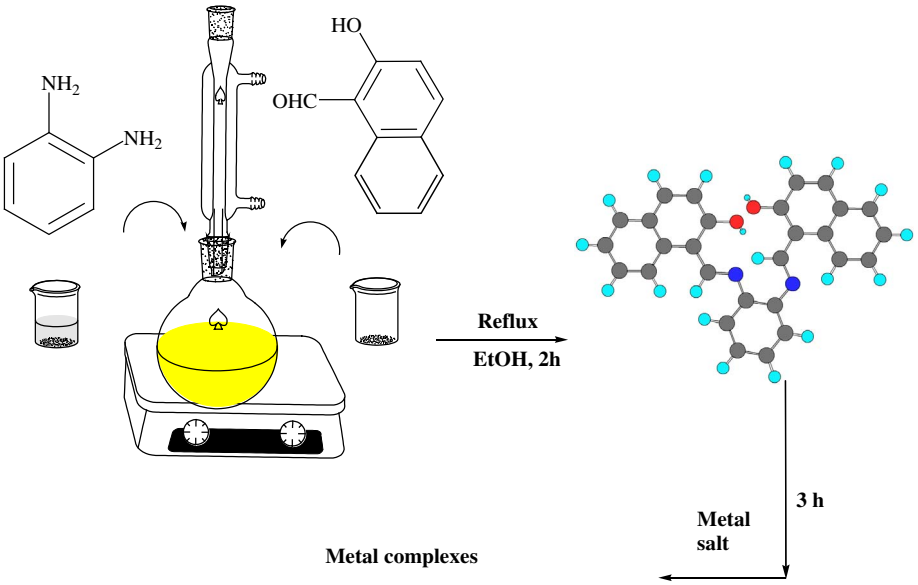

Scheme 1. Synthetic strategy for the preparation of the investigated complexes.

solid was filtered off from the reaction mixture, thoroughly washed with ethanol and desiccated over anhydrous $CaCl_2$. The purity of the complexes was checked by TLC.

^{1}HNMR (δ, ppm), in DMSO (HNPNNi complex): 9.41(s, 2H, 2CH=N), 8.53 (d, 2H), 8.45:6.50 (m, 14H, aromatic) (cf. Fig. S3).

2.4. Evaluation of the Stoichiometry of the Prepared Imine Complexes

The molar ratio [11–15,19–21] and continuous variation methods [11–15,19–21] were used to study the equilibria in solutions and to determine M:L ratio .

2.5. Evaluation of the Apparent Formation Constants of the Investigated Complexes

The formation constants (K_f) of the studied Schiff base metal complexes formed in solutions were obtained from the spectrophotometric measurements by using the continuous variation method [11–15,19–22] in Table 6 according to the following relation.

$$K_f = \frac{A/A_m}{(1 - A/A_m)^2 C} \quad (1)$$

where, A_m is the absorbance at the maximum formation of the complex, A is the spot chosen absorbance values on either side of the absorbance mountain col. (pass) and C is the initial concentration of the metal. Also, the free energy change, $\Delta(G^*)$ of the complexes was determined by $\Delta(G^*) = -RT \ln K_f$, at 25 °C where K_f, is the formation constant, R is the gas constant and T is the temperature in Kelvin.

2.6. Kinetic Studies

The kinetic parameters of decomposition process for metal complexes were extracted from Coast-Redfern integral method [19–22]. The thermodynamic parameters such as the energy of activation (E^*) the entropy of activation (ΔS^*), enthalpy (ΔH^*) and free energy change (ΔG^*) of the decomposition of the metal complexes by employing the following equation,

$$\log\left[\frac{\log(w_\infty/(w_\infty - w)}{T^2}\right] = \log\left[\frac{AR}{\phi E^*}\left(1 - \frac{2RT}{E^*}\right)\right] - \frac{E^*}{2.303RT} \quad (2)$$

where w_∞ is the mass loss at the completion of the decomposition reaction, w is the mass loss up to temperature T, R is the universal gas constant and ϕ is the heating rate. Since 1-2RT/E* ≈ 1. A plot of the left-hand side of Eq. (1) against 1/T gives a slope from which E^* was evaluated and A was determined from the intercept. The other kinetic parameters; the entropy of activation (ΔS^*), enthalpy of activation (ΔH^*) and the free energy change of activation (ΔG^*) were evaluated using the following expression [21,22]:

$$\Delta S^* = 2.303R \log \frac{Ah}{K_B T} \quad (3)$$

$$\Delta H^* = E^* - RT \quad (4)$$

$$\Delta G^* = H^* - T\Delta S^* \quad (5)$$

where (K_B) and (h) are Boltzmann's and Plank's constants, respectively.

2.7. Biological Studies

2.7.1. Antibacterial and Antifungal Activity Screening

The in vitro biological activity of the presented HNPN imine ligand and its complexes were examined against different types of bacteria (*Bacillus subtilis (+ ve)*, *Escherichia coli (− ve)* and *Staphylococcus aureus (+ ve)*) by well diffusion method using nutrient agar as the environment [21–23]. The antifungal actions of the compounds were also tested by the well diffusion route against different types of fungi (*Aspergillus niger*, *Candida glabrata* and *Trichophyton rubrum*) on potato dextrose agar as environment. The complexes have been dissolved in DMSO and the solutions of concentrations 10 and 20 (mg/ml) were prepared separately. In a typical method, a well was made on the agar medium inoculated with micro-organism [21–23]. The well was full of the test solution utilizing a micropipette and the plate was incubated 24 h at 37 °C for the bacteria or 72 h at 30 °C for the fungi. After incubation, the diameter of the obvious zone of inhibition around the sample was taken as a standard for the inhibitory power of the sample against the specific check organism. The first tube without turbidity was evaluated as the minimum inhibition concentration (MIC) (mg/ml). Gentamycin was used as positive control for bacteria and Fluconazol was used as positive control for fungi. The sensitivity was registered by measuring the clear zone of growth inhibition of agar surface around the well in millimeter. In order to clarify the effect of solvent (DMSO) on the biological screening, DMSO alone was used as control, and it showed no activity against microbial strains. The measurements were made in triplicate for each compound and their average values are determined.

2.7.2. DNA Binding Study

Calf thymus DNA(CT-DNA), bromophenol blue dye, ethidium bromide and Tris[hydroxymethyl]-aminomethane(Tris)were achieved from (Sigma-Aldrich Chemie (Germany)).

All the tests involving the interaction of the complexes with DNA were rolled in Tris–HCl buffer (60 mM, pH 7.1). CT-DNA was purified by centrifugal dialysis before using. A solution of calf thymus DNA in the buffer offered a ratio of UV absorption at 260 and 280 nm of about > 1.85, indicating that the DNA was sufficiently free from protein contamination [21–23]. The concentration of DNA was evaluated by monitoring the UV absorbance at 260 nm utilizing $\varepsilon_{260} = 6600\ mol^{-1}\ cm^2$. The stock solution was saved at 4 °C and used within only one day.

2.7.2.1. Electronic Spectra of Interaction with DNA. Spectrophotometric titration experiment was carried out keeping the complex concentration constant while altering the nucleic acid concentration in the interaction environment. The absorption due to free CT-DNA was separated by accession an equimolar CT-DNA to pure buffer solution in the reference compartment and the forming spectra were considered to result from the complexes and the DNA–metal complex assemblages [5,11,15]. From the absorption data, the intrinsic binding invariable (K_b) was determined by plotting [DNA] / ($\varepsilon_a - \varepsilon_f$) vs. [DNA] according to the following equation:

$$\frac{[DNA]}{(\varepsilon_a - \varepsilon_f)} = \frac{[DNA]}{(\varepsilon_b - \varepsilon_f)} + \frac{1}{[K_b(\varepsilon_b - \varepsilon_f)]} \quad (6)$$

where, [DNA] is the concentration of DNA in base pairs, ε_a, ε_f and ε_b are the apparent, free and fully bound complex extinction coefficients, respectively. In particular, ε_f was evaluated from the calibration curve of the isolated metal complex; verifying the Beer's law. ε_a was evaluated as the ratio between the determined absorbance and the M(II) complex concentration, A_{obs} / [complex]. The data were suitable for the above equation with a slope equal to 1 / ($\varepsilon_b - \varepsilon_f$) and y-intercept equal to 1 / [$K_b(\varepsilon_b - \varepsilon_f)$] and K_b was obtained from the ratio of slope to intercept. The standard Gibbs free energy for DNA binding was estimated from the following relation [5,11,21–23]:

$$\Delta G_b^{\neq} = -RT \ln K_b \quad (7)$$

2.7.2.2. Viscosity Experiments. Viscosity measurements were carried out using an Oswald micro viscometer, protected at constant temperature at 25 °C. The fluidity times were recorded for various concentrations of the complex (5–50 μM), maintaining the concentration of DNA constant (260 μM). Mixing of the solution was achieved by bubbling the nitrogen gas through the viscometer. The mean value of the three measures was used to determine the viscosity of

the samples. The buffer fluidity time in seconds was recorded as t°. The relative viscosities for DNA in the presence (η) and absence (η°) of the complex were evaluated utilizing the relation $\eta = (t - t^{\circ}) / t^{\circ}$. Where, t is the recorded fluidity time in seconds and the amounts of the relative viscosity (η/η°) were plotted against 1/R (R = [DNA] / [Complex]) [5,11,19,21–23].

2.7.2.3. Agarose Gel Electrophoresis. The DNA binding products were checked by agarose gel electrophoresis method [19]. The stock solution of complexes was prepared by dissolving 20 mg of the compounds in 20 ml of DMF. The sample (25 μg/ml) was added to the separated DNA of Calf-thymus (CT-DNA) and incubated for 1 h at 37 ± 1 °C and then 30 μl of DNA sample (mixed with bromophenol blue dye at a 1:1 ratio) was charged on attention into the electrophoresis chamber wells along with a standard DNA marker in TBE buffer (50 mM Tris base, pH 7.2; 1 mM EDTA/1 l) and then loaded onto the agarose gel, then a constant electricity (60 V) was left for about 45 min. Finally, the gel was removed and stained with 20 μg/ml of ethidium bromide for 10–20 min. The bands obtained was monitored under UV light using a transilluminator directed by photography with DMC-LZ5 Lumix Digital Camera to determine the extent of DNA binding as compared with standard DNA marker [5,21–23].

2.7.3. Anticancer Activity

The anticancer activity was made at the National Cancer Institute, Cancer Biology Department, Pharmacology Department, Cairo University. The absorbance or optical density (O.D.) of each well was estimated spectrophotometrically at 564 (nm) with an "ELIZA" micro plate reader (Meter tech. Σ 960, "USA"). Evaluation of the cytotoxic activity of the prepared ligand and its complexes was carried out against Colon carcinoma cells, (HCT-116 cell line) and Breast carcinoma cells, (MCF-7 cell line). The evaluation process was carried out in vitro using the Sulfo-Rhodamine-B-stain (SRB) [5,12]. Cells were placed in 96-multiwell plate (10^4 cells/well) for 24 h before processing with the complexes to allow attachment of cell to the wall of the plate. Various concentrations of the investigated compounds in DMSO (0, 1, 2.5, 5 and 10 μM) were added to the cell monolayer. Monolayer cells were incubated with the complexes for 48 h at 37 °C and in atmosphere of 5% CO_2. After 48 h, cells were fixed, rinsed, and stained with Sulfo-Rhodamine-B-stain [5,12,23]. Excess stain was washed with acetic acid and attached stain was administered with Tris EDTA buffer. Color intensity was measured in an ELISA reader. IC_{50} was evaluated and potency was calculated with regard to percentage of change of (vistabline standard) [5,12,24]. The inhibitory concentration percent (IC %) was estimated [5,12,23,25] according to the equation: Inhibition concentration.

$$(IC)\% = (\text{Control O. D.} - \text{Ligand O. D.}) \times 100/\text{Control O. D.} \quad (8)$$

2.8. Molecular Docking Study

Docking stimulation study is performed using molecular operating environment (MOE®) version 09.2014, Chemical Computing Group Inc., Montreal, Canada. The computational software operated under "Windows XP" installed on a Intel Pentium IV PC with a 1.6 GHz processor and 512 MB memory [26].

Firstly, a Gaussian Contact surface around the binding site was sketched, then the surface enclosed the *van Waals* surface. Finally docking studies were done to assess the binding free energy of the inhibitor inside the macromolecule. The scoring in docking studies was done utilizing London dG scoring function. Each docking experiment was derived from 10 different runs were directed to analyze or achieving the best score. To compare the docking belonged to the ligand in the co-crystallized structure and to obtain RMSD of the docking pose database browser was used.

2.8.1. Preparation of Ligands and Target Protein-Tyrosine Kinase

The compounds in this research as ligands were studied for their binding ability into protein-tyrosine kinase (TRK). The target compounds were constructed into a 3D model using the builder interface of the MOE program after checking their structures and the formal changes on atoms by 2D depiction, the following steps were carried out: The target compounds were subjected to a conformational search. Conformers were subjected to energy minimization using MOE module until a RMSD gradient of 0.01 and RMS distance of 0.1 A° Kcal mol^{-1} $A^{\circ -1}$ with MMFF94X force-field and the partial charges were automatically evaluated. The obtained database was then saved as MDB file to be used in the docking calculations. The X-ray crystallographic structure of c-kit receptor protein-tyrosine kinase in complex with STI-571 (Imatinib or Gleevec) were uploaded from the Protein Date Bank (PDB) (http://www.rcsb.org/pdb/explore/explore.do?structureId=1T46) (PDB code: 1t46) was obtained from Protein data bank [27]. Partial charges and hydrogen atom were put on to the protein with the protonation 3D application in MOE. This application is carried out to appropriate position hydrogen atom in the macromolecule structures and ionization states. Then four steps were made for both active sites: checking the atoms connection and type, adding hydrogen atoms to the system, selection of the receptor an fix it's atoms potential, MOE Alpha Site Finder was used for the active site search in the enzyme structure using all default items. The active site was chosen to contain the residues that were bound to receptor. Dummy atoms were created from the obtained alpha Spheres.

2.8.2. Molecular Modeling and Analysis of the Docked Results

The binding affinity of the synthesized compounds to TRK protein by formation of the hydrogen bonds between the ligand and amino acid in TRK were carried out, which measured the hydrogen bond length, which does not surpass 3.7 A°. In addition, RMSD of the co-crystal ligand position compared to the docking pose was used in ranking. Both RMSD as well as the mode of interaction of the regional ligand within the crystal structure of c-kite tyrosine kinase receptor were carried out as the standard model.

3. Results and Discussion

3.1. Physicochemical Properties of the Prepared HNPN Imine Ligand and Its Complexes

3.1.1. ^1H NMR and ^{13}C-NMR Spectra

The ^1H NMR spectral data of the prepared HNPN imine ligand and HNPNNi complex were recorded in the experimental section. The ^1H NMR spectrum of HNPN imine ligand exhibited singlet signal at δ = 15.05, that are assigned to the two phenolic −OH group. The signal due to the two azomethine protons (−HC═N) is found to be at δ = 9.69 ppm [28]. The signals due to aromatic protons of 2-hydroxynapthaldehyde and *o*-phenylenediamine have resonated as multiplets in the region of 8.11–7.05 ppm of 14H protons. It also shows two protons doublet at position 10.

^1H NMR spectrum of the prepared HNPNNi complex has a shift in signals for CH═N protons compared to HNPN ligand confirm its chelation to Ni(II). Also the disappearance of signal due to phenolic −OH confirm that the deprotonating of it when coordinated with Ni(II).

3.1.2. Elemental Analyses and Conductivity Data

All the prepared complexes are tinted, solid, steady at room temperature and non-hygroscopic in nature. The analytical and physicochemical data of ligand and its complexes are listed in Table 1 confirm the proposed structures of the ligand and its complexes. The metal complexes exhibit 1:1 (metal-ligand) stoichiometry.

The molar conductance of all investigated complexes was observed at room temperature in DMF as a solvent and their results in (Ω^{-1} cm^2 mol^{-1}) are recorded in Table 1. The molar conductance

Table 1
Analytical and physical data of the prepared HNPN imine ligand and its complexes.

Compounds (molecular formula)	M. wt	Color yield (%)	Λ_m (Ω^{-1} cm^2 mol^{-1})	μ_{eff} (B.M.)	M.p and dec. temp (°C)	Analysis (%) found (calcd.)		
						C	H	N
HNPN	416.50	Black yellow	–		160	80.56	4.74	6.79
$C_{28}H_{20}N_2O_2$		(92)		–		(80.67)	(4.80)	(6.72)
HNPNCr	582	Deep brown	5.70	3.81	(> 300)	57.68	4.09	7.19
$C_{28}H_{24}N_3O_8Cr$		(88)				(57.73)	(4.12)	(7.22)
HNPNMn	504.94	Deep brown	12.50	4.77	(210)	66.43	4.32	5.49
$C_{28}H_{22}MnN_2O_4$		(89)				(66.54)	(4.36)	(5.56)
HNPNNi	490.69	Red	7.40	Dimag.	(> 300)	68.54	4.12	5.77
$C_{28}H_{20}NiN_2O_3$		(87)				(68.48)	(4.08)	(5.71)
HNPNV	489.94	Brait	5.90		(> 300)	68.69	3.92	5.79
$C_{28}H_{19}N_2O_{3.5}V$		(83)		1.82		(68.58)	(3.88)	(5.71)

Table 2
Characteristic IR bands of the prepared HNPN imine ligand and its complexes.

Compounds	υ)OH)/ H2O	υ)CH)ar	υ(C═N (vs))	υ) C—O) ph	υ(M—N)	υ(M—O)
HNPN	3423 (s)	3048	1622	1250 (m)	–	–
HNPNCr	3426	3082 (s)	1610 (s)	1186	451(m)	569 (w)
HNPNMn	3382 (m)	3028 (m)	1617 (s)	1192 (m)	475	565
HNPNNi	3423 (s)	3051 (m)	1604 (s)	1196 (m)	429 (w)	565 (m)
HNPNV	3444 (s)	3034 (m)	1614 (s)	1193 (w)	417 (m)	559 (m)

vs = very strong, s = strong, m = medium, b = broad, w = weak, ar = aromatic, py = pyridine, ph = phenolic, asy = asymmetric, sy = symmetric.

values of all the metal complexes at room temperature fall into the higher range (5.7–12.50 Ω^{-1} cm^2 mol^{-1}) assigned to their nonelectrolytic nature.

3.1.3. Infrared Spectra

The bonding of the prepared HNPN imine ligand to the metal ions has been judged by a careful comparison of the infrared spectra of the metal complexes with those of the free ligand. The characteristic IR frequencies of the HNPN ligand its complexes along with their assignments are shown in Table 2. Bands due to −OH and −CH═N are distinguishable and offer proof regarding the structure of the ligand and its bonding with metal. A band at 1622 cm^{-1} in the HNPN ligand is due to −C═N stretching vibration. On complexation, this band is displaced to a lower frequency (1604–1610 cm^{-1}). The negative shift of this band is an obvious indication of the involvement of the azomethine nitrogen atoms in complex formation [12–15,29,30].This is supported by the appearance of band at 451–470 cm^{-1} corresponding to the stretching vibration of M—N bond. Bands at 569–559 cm^{-1} correspond to M—O stretching vibrations. Band at 3423 cm^{-1} observed in the ligand spectrum is due to stretching vibrations of free –OH. In the complexes, the recorded IR spectra of all the prepared imine complexes show broad band at 3444–3383 cm^{-1} which have been referred to υ(OH) stretching vibration of crystalized water molecules, in accordance with the findings of the elemental analysis listed in Table 2. A band at 968 cm^{-1} (OH rocking) suggests the presence of coordinated water in HNPN complex. In the low frequency region, the band founded in HNPN imine ligand showed an absorption band at 1250 cm^{-1} which can outcome from the stretching vibration of the phenolic (C—O) group. The shifting of that band to lower wave number values onto coordination shows that the oxygen atoms of the phenolic groups are coordinated to the metal ion. The characteristic frequencies of the coordinated nitrate group in HNPNCr complex possess three non-degenerated modes at 1472 cm^{-1} υ(NO_2)asy, 1352 cm^{-1} υ(NO_2)sy and 855 cm^{-1} υ(NO) [31].

3.1.4. Electronic Spectra

The molecular electronic absorption spectra are often very significant in the evaluation of results furnished by other methods of structural check. The electronic spectral measurements were utilized to assign the stereo chemistries of metal ions in the complexes depending on the sites and number of *d–d* transition peaks [32].The electronic absorption spectra of ligands and their complexes were listed at the wavelength range 800–200 nm and at 298 K. The ligand exhibits absorption bands in UV–Vis region around 392 nm which is assigned to n → π* transition originating from the imine function of the Schiff base ligand [12–15].The absorption bands of complexes at λ_{max} = 361–464 nm is assigned to charge transfer from Schiff base ligand to metal ion (cf. Fig. 1 and Table S1) Furthermore, A long and a broad band lying in the region 481–557 nm. This band could be mainly attributed to the *d* → *d* transition in the structure of the prepared complexes (cf. Table S1) [12–15,32].

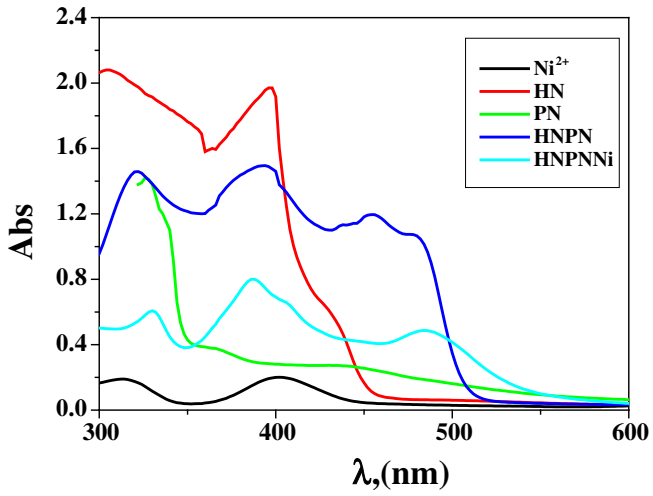

Fig. 1. Molecular electronic spectra of 10^{-3} M of HNPNNi complex and its components (Ni^{2+} ion, 2-hydroxynapthaldehyde(HN), o-phenylenediamine (PN), and HNPN imine ligand) in DMF at 298 K.

3.1.5. Magnetic Moment Measurements

The diamagnetic complexes will be repelled in a magnetic field while the paramagnetic complexes will be attracted. For paramagnetic materials, the flux is greater within the substance than it would be in vacuum. Therefore, paramagnetic materials have positive susceptibilities. Thus, the magnetic susceptibility measurements offer information considering the geometric structure of the compounds. The magnetic susceptibility of VO(II) complexes have a magnetic moment value of 1.82 B.M., which is close to the spin-only value for d^1 and in agreement with the reported values for square pyramidal octahedral complexes of VO(II) [33]. While, in case of HNPNMn complex, the imine ligand is so strong that it exhibited high t_2g and e.g. d-splitting of the octahedral structures of the complexes. Thus, HNPNMn is low spin inner complex.

Table 3
Thermal decomposition steps, mass loss (%), proposed lost segments, final residue thermo-kinetic activation parameters of each decomposition step for the prepared complexes.

Complex	Decomp. temp. (°C)	Mass loss (%)		Proposed segment	E^* (kJ mol^{-1})	A (S^{-1})	ΔH^* (kJ mol^{-1})	ΔG^* (kJ mol^{-1})	ΔS^* (J mol^{-1} K^{-1})
		Found	(Calc.)						
HNPNCr	41–116	6.13	6.19	$2H_2O$		0.08	87.7	107.8	− 254.9
	118–220	3.03	3.09	H_2O	88.4		87	131.1	− 261.2
	222–295	10.59	10.65	NO_3			86	154.8	− 264.8
	297–411	29.07	29.04	$C_{11}H_7NO$			85	179.6	− 267.4
	413–597	42.07	42.1	$C_{17}H_{11}NO$			84	220.5	− 270.34
Residue	> 597	8.93	8.9	Cr			–	–	–
HNPNMn	31–116	6.54	(6.66)	$2H_2O$	64	0.11	63.3	83.2	− 252.3
	116–200	6.61	(6.66)	$2H_2O$			62.7	103.5	− 258.03
	200–375	31.17	(31.24)	$C_{11}H_7NO$			61.6	137.6	− 263.05
	375–528	45.26	(45.29)	$C_{17}H_{11}NO$			60	180.9	− 266.78
Residue	> 528	10.09	(10.15)	Mn			–	–	–
HNPNNi	32–115	3.53	(3.67)	H_2O	31.5	0.066	30.98	46.7	− 249.97
	223–381	34.37	(34.44)	$C_{11}H_7NO$			28.9	110.6	− 268.1
	384–595	50.11	(49.9)	$C_{17}H_{11}NO$			27.4	162.5	− 271.80
Residue	> 595	12.03	(11.96)	Ni			–	–	–
HNPNV	30–120	1.83	(1.84)	$0.5H_2O$	15.6	0.025	15	33.5	− 263.58
	122–518	34.52	(34.49)	$C_{11}H_7NO$			12.9	101.3	− 276.2
	520–797	50.13	(50.01)	$C_{17}H_{11}NO$			10.1	197.3	− 282.3
Residue	> 797	13.53	(13.66)	VO			–	–	–

HNPNCr complex shows magnetic moment corresponding to three unpaired electrons, i.e. (3.81 B.M.), as expected for high- spin octahedral Cr(III) complexes. HNPNNi complex has no magnetic moment and this indicates that HNPNNi complex is diamagnetic with square planar geometry (cf. Table 1).

3.1.6. Thermal Analysis

The first stage in the decomposition process of HNPNMn complex is related to dehydration of two water molecules at 116 °C with mass loss (found 6.54%, calc. 6.66%). The second step corresponds to elimination of the two coordinated water molecules with mass loss (6.61%, Calc.6.66%). The third and fourth steps are the removal of organic moiety with mass losses (found 31.17%, calc. 31.24%) and (found 45.26%, calc. 45.29%) . Finally metallic residue is the final product of thermal decomposition with mass losses (found 10.09%, calc. 10.15%) (cf. Table 3).

The TGA of HNPNNi complexes showed a loss in weight at 115 °C, indicating the elimination of lattice one water molecule with mass loss (found 3.53%, calc. 3.67%) [34]. The second stage corresponds to a mass loss of (found 34.37%, calc. 34.44%) within the temperature ranges 117–381 °C represents the loss $C_{11}H_7NO$ as a part of ligand. The third stage corresponds to the removal of final part of ligand $C_{17}H_{11}NO$ at temperature up to 595 °C leaving metallic residue Ni [22]. These results are in consistent with the composition of the complex.

The TGA of HNPNV complexes showed a loss in weight within the range from 30 to 120 °C, indicating the elimination of lattice half water molecule with mass loss (found 1.83%, calc. 1.84%) [34]. The second and third step correspond to a mass losses of $C_{11}H_7NO$ and $C_{17}H_{11}NO$ of the ligand (found 34.52%, calc. 34.49%) and (found 50.13%, calc. 50.01%) within the temperature ranges 122–518 °C and 122–518 °C 520–797 °C, respectively leaving VO(II) as a residue.

The thermogram of HNPNCr complex exhibited five decomposition steps within the temperature range 40–597 °C. The first step correspond to elimination of two lattice water molecules with mass loss of (found 6.13%, calc. 6.19%). The second step of decomposition within the temperature range 118–220 °C corresponds to the loss of one coordinated water molecule, with a mass loss of 3.03% (Calc. 3.09%). The third step 222–295 °C corresponds to the loss of nitrate group (NO_3) with a net weight loss of 10.59% (Calc. 10.65%).

The fourth and fifth steps are consistent with elimination of organic matter ($C_{11}H_7NO$, $C_{17}H_11NO$) with mass losses (found 29.07, calc. 29.04%) and (found 42.07, calc. 42.10%) within the temperature ranges 297–411 °C and 413–597 °C, respectively leaving Cr as a metallic residue [14,35].

3.1.6.1. Kinetic Aspects. The Kinetic parameters are shown in Table 3. It is shown that G* values increase due to increase temperature. The positive values of H* explain that degradation processes are endothermic. In most thermal steps, S* values are negative suggesting a degradation via abnormal pathway at those steps and the degradation processes are undesirable. The negative activation entropy values give evidence for a more ordered activated state. This can be proper through the chemisorption of oxygen and other decomposition products. The nature of the more ordered can attributed to the bonds polarization of the activated state which occurs through electronic transitions. Finally, positive values of H* and G* representing the endothermic character for all thermal steps [36] (cf. Table 3).

3.1.7. Spectrophotometric Determination of the Stoichiometry of the Prepared Complexes

Stoichiometry of the prepared complexes is determined using the two methods including the use of spectrophotometry, namely, continuous-variations method [37–40] and molar-ratio method. Based on the

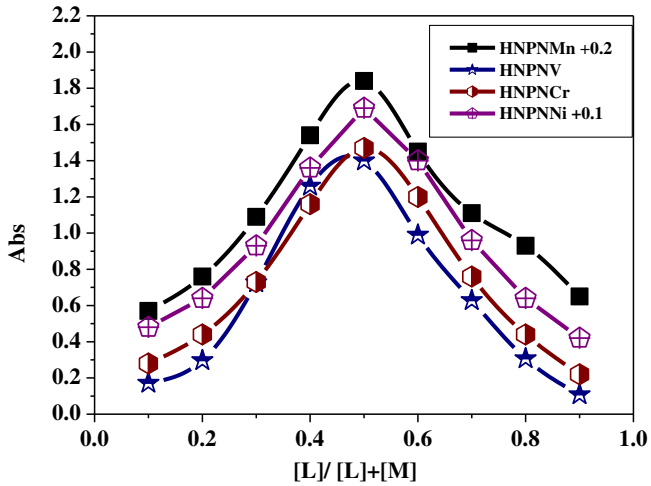

Fig. 2. Continuous variation plots for the prepared HNPNMn, HNPNV, HNPNNi and HNPNCr complexes in aqueous–ethanolic medium at [HNPNCr] = [HNPNNi] = [HNPNV] = [HNPNMn] = 10^{-3} M and 298 K.

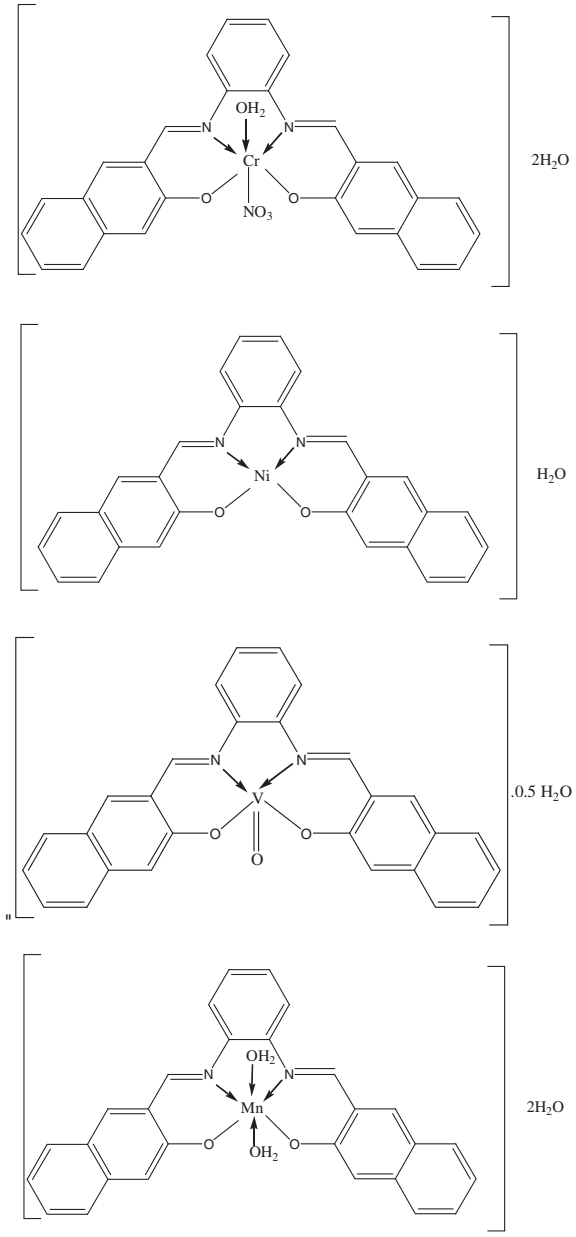

Scheme 2. The suggested structures of the investigated complexes.

Table 4
The formation constant (K_f), stability constant (pK) and Gibbs free energy Δ(G*) values of the synthesized complexes at 298 K.

Complex	Type of complex	K_f	Log K_f	ΔG^* (kJ mol^{-1})
HNPNMn	1:1	1.07×10^4	4.03	− 22.99
HNPNV	1:1	1.66×10^4	4.22	− 24.07
HNPNCr	1:1	1.39×10^4	4.14	− 23.64
HNPNNi	1:1	1.09×10^4	4.04	− 23.03

obtained results, the stoichiometry of the prepared complexes is 1:1. The curves of the continuous variation method (cf. Fig. 2) displayed maximum absorbance at mole fraction X_{ligand} = 0.5–0.6 showing the complexation of metal ions to ligand in molar ratio 1:1. Moreover, the data resulted from using the molar ratio method support the same metal ion to ligand ratio of the prepared complexes (cf. Fig. S4 and Scheme 2) [11–15,24].

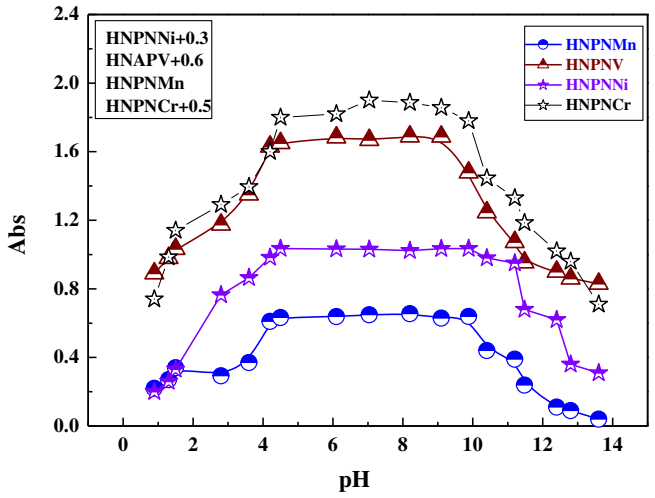

Fig. 3. Dissociation curve of the prepared imine HNPNMn, HNPNV, HNPNNi and HNPNCr complexes in DMF.

3.1.7.1. Determination of the Apparent Formation Constants of the Synthesized Complexes. The formation constants (K_f) of the studied imine complexes formed in solution were obtained from the spectrophotometric measures by utilizing the continuous variation method (cf. Table 4). As mentioned in Table 4, the obtained K_f values show the high stability of the tested complexes. The values of K_f for the checked complexes increase in the following order: HNPNV > HNPNCr > HNPNNi > HNPNMn complex. Moreover, The stability constant(pK) and Gibbs free energy ($\Delta G^{\neq}$) values of the presented complexes are calculated. The negative values of Gibbs free energy show that the reaction is spontaneous and favored. The pH-profile (absorbance vs. pH) explained in (cf. Fig. 3) showed typical dissociation curves and a high stability pH extent (4–9) of the tested complexes. This implies that the formation of the complex greatly stabilizes the prepared imine ligand [5,11–15,22,24]. Consequently, the desired pH range for the different applications of the tested complexes is from pH = 4 to pH = 9. Based on obtained results of elemental analyses, molar conductance, magnetic measures, infrared and electronic spectra, the suggested composition of the complexes was identified.

3.2. Antimicrobial Activity Evaluation

The in vitro antimicrobial actions of the HNPN imine ligand and its complexes against three selected bacteria *Escherichia coli (− ve)*, *Bacillus subtilis (+ ve)* and *Staphylococcus aureus (+ ve)*) and three fungi (*Aspergillus flavus*, *Candida albicans and Trichophyton rubrum),*were determined. Any chemotherapeutic agent inhibits the growth of microbes by microstatic mechanisms. All the investigated compounds displayed good biological activity with the micro-organism. On contrasting the biological wares of the titled imine ligand, its complexes with those of a standard bactericide and fungicide, it was clear that the complexes had moderate activity as matched with the standard, but all the complexes were more active than free titled ligand. The higher inhibition zone of the transition metal complexes than those of the titled ligand can be shown based on the Overtone notion and the chelation theory. Upon chelation, the polarity of the metal ion is reduced to a great extent due to the overlap of the ligand orbital and the fractional participating of the positive charge of the metal ion with donor groups. Furthermore, it promotes the delocalization of the π-electrons over the whole chelating ring and increases the breakthrough of the complexes into lipid membranes and the blocking of the metal attachment locations in the enzymes of micro-organisms [5,11–15,24]. The conclusions of the investigations account for the antipathogenic manner of the compounds and this efficacy is positively changed on

Table 5
Results of antibacterial and antifungal bioassay of the prepared HNPN imine ligand and its complexes against different strains of bacteria and fungi.

Compounds	Inhibition zone (mm)											
	Escherichia coli (− ve)		*Bacillus subtilis (+)*		*Staphylococcus aureus (+ve)*		*Candida albicans*		*Aspergillus flavus*		*Trichophyton rubrum*	
Conc. (mg/ml)	10	20	10	20	10	20	10	20	10	20	10	20
HNPN	4 ± 0.44	11 ± 0.57	6 ± 0.18	14 ± 0.14	5 ± 0.74	12 ± 0.55	5 ± 0.22	7 ± 0.68	3 ± 0.29	7 ± 0.41	3 ± 0.19	6 ± 0.51
HNPNV	15 ± 0.39	32 ± 0.59	20 ± 0.06	42 ± 0.11	16 ± 0.26	34 ± 0.16	13 ± 0.15	22 ± 0.92	8 ± 0.81	19 ± 0.12	8 ± 0.59	14 ± 0.77
HNPNMn	13 ± 0.70	27 ± 0.10	14 ± 0.62	35 ± 0.43	12 ± 0.86	29 ± 0.08	12 ± 0.10	20 ± 0.91	7 ± 0.82	17 ± 0.02	7 ± 0.16	13 ± 0.12
HNPNNi	14 ± 0.03	31 ± 0.80	18 ± 0.45	41 ± 0.40	14 ± 0.57	33 ± 0.25	15 ± 0.15	26 ± 0.62	9 ± 0.20	21 ± 0.50	9 ± 0.37	16 ± 0.41
HNPNCr	16 ± 0.20	33 ± 0.36	19 ± 0.30	40 ± 0.17	15 ± 0.50	32 ± 0.48	14 ± 0.21	25 ± 0.23	10 ± 0.62	22 ± 0.12	8 ± 0.62	15 ± 0.10
Gentamycin	20 ± 0.71	40 ± 0.33	26 ± 0.15	51 ± 0.72	25 ± 0.93	45 ± 0.11	24 ± 0.55	37 ± 0.62	16 ± 0.49	31 ± 0.88	15 ± 0.71	25 ± 0.90
Fluconazol												

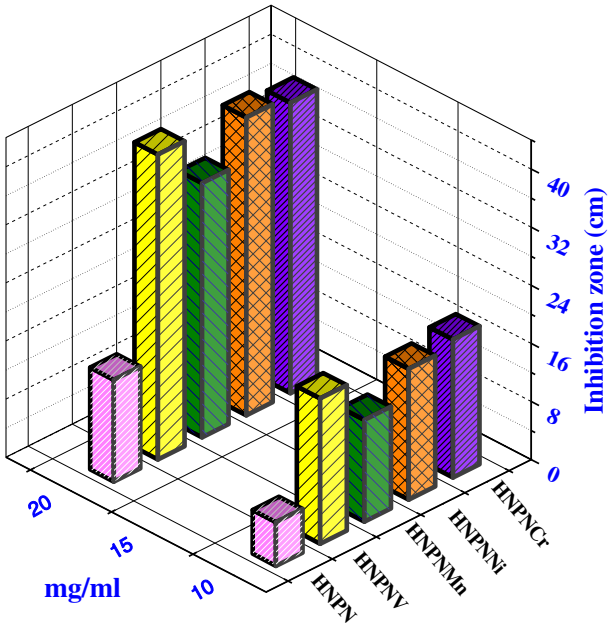

Fig. 4. Histogram showing the comparative antibacterial activities of the prepared compounds (HNPN, HNPNCr, HNPNNi, HNPNMn and HNPN V) against *B. subtilis* bacteria.

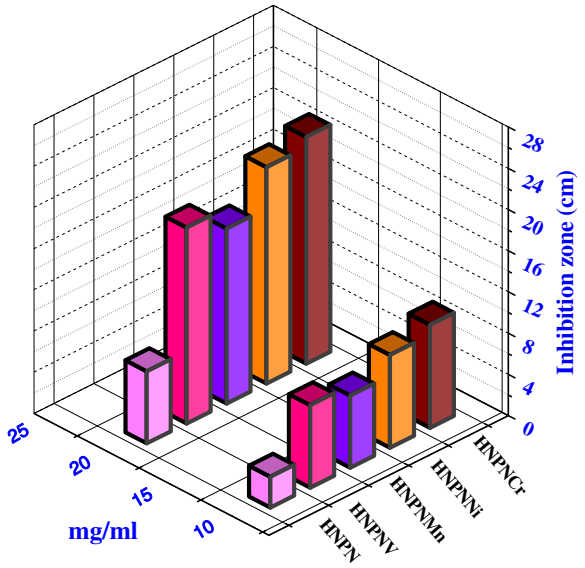

Fig. 5. Histogram showing the comparative antifungal activities of the prepared compounds (HNPN, HNPNCr, HNPNNi, HNPNMn and HNPNV) against *A. flavus* fungi.

complexation. Data are listed in Table 5 and Figs. 4, 5. The minimum inhibitory concentration (MIC) (mg/ml) was estimated by serial dilution route and reported in Table 6. The HNPNV complex (3 mg/ml) was found to be highly effective as they exhibit the lowest MIC against *Bacillus subtilis* bacteria *and Candida albicans* fungi compared to other prepared compounds. The antimicrobial studies suggested that all the complexes exhibited safely promoted antimicrobial activity against microbial strains in comparison to the free ligand. Previous studies elsewhere suggested that chelation tended to make the ligand have more powerful and potent bacteriostatic agents [14,15,22,23], thus inhibited the growth of microbe more than the ligand. It was showed that factors such as solubility, conductivity, dipole moment, and cell permeability technique influenced by the presence of metal ion might

Table 6
Minimum inhibition zone (MIC, mg/ml) for antimicrobial assay of the prepared HNPN imine ligand and its complexes.

Compounds	Bacteria			Fungi		
	S. aureus	*B. subtilis*	*E. coli*	*A. flavus*	*C. albicans*	*T. rubrum*
HNPN	9	7.5	8	7	5.5	6
HNPNV	5	3	4	5	3	4.5
HNPNMn	5	5	5.5	5.5	3	4.5
HNPNNi	5	4	4.5	3.5	4.5	4
HNPNCr	4.5	4	5	4	5	4.5

be the possible reason for the increase in activity. The activities of the prepared complexes were confirmed by calculating the potency index (cf. Table S2) according to the following relation [5,11–15,22,23]:

$$\text{Activity index(A)} = \frac{\text{inhibition zone of complex(mm)}}{\text{inhibition zone of standard drug(mm)}} \times 100 \quad (9)$$

The variation in the activity of the metal chelates against different microbes depend either on the difference in the impermeability of the cells of the microbes or on the ribosomes of the microbial cells. The lower activity of complexes as compared to others may be rationalized to low lipid solubility, so that the metal ion may not be able to reach the favorable site of action of the cell wall to get interfere with the normal cell activity. Although chelation itself plays a significant role in determining antibacterial behavior of the complexes but concurrently different factors such as solubility, coordinating sites, size, dipole moment, redox potential of metal ion, solubility, bond length between metal and the ligand, pharmacokinetic, geometry of complexes, steric, concentration and hydrophobicity have substantial influence on the antibacterial activity. Thus, it is apparent from the results that enhanced antibacterial activity of the metal complexes may not be only due to chelation but also intricate integrations of several other factors as well [14,15].

3.3. Binding Potency

3.3.1. Electronic Spectra of Interaction With DNA

Titration with electronic absorption spectroscopy is an active route to check the binding mode of DNA with metal complexes. The spectra were registered as a function of the addition of the buffer solutions of pure CT-DNA to the buffer solutions of the tested complexes (Table 7). If the interaction mode is intercalation, the orbital of the inserted ligand can couple with the orbital of the base pairs, lowering the π–π* transition energy and lead to bathochromism. If the conjunction orbital is partially filled by electrons, it reduces the transition probabilities and lead to hypochromism [5,11–15]. The extent of the hypochromism or hyperchromism in the charge transfer from metal-to-ligand (MLCT) band is commonly consistent with the force of intercalation interaction [12–25,24]. The electronic absorption spectra of HNPNCr complex in the absence and presence of various concentrations of buffered CT-DNA are given in Figs. 6, S5. Addition of increasing amounts of CT-DNA resulted in a reduction of absorbance for a complex. The spectral parameters and Kb for the DNA interaction with the tested complexes are shown in Table 6. The investigated complexes could bind to DNA mainly via an intercalative and replacement modes with the sequence: HNPNCr > HNPNNi > HNPNV > HNPNMn complex (cf. Scheme 3a).

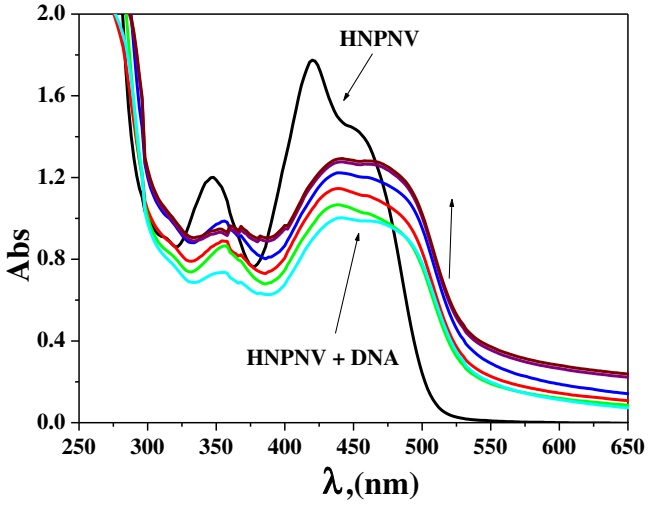

Fig. 6. Spectral scans of the interaction of HNPNV complex (10^{-3} mol dm^{-3}) in 0.01 mol dm^{-3} Tris buffer (pH 7.2, 298 K) with CT-DNA (0 − 30) μM DNA, from top to bottom.

3.3.2. Viscosity Measurements

For explaining the interaction nature between the tested complexes and DNA, viscosity measures were carried out. Hydrodynamic methods like a viscosity measures which are sensitive to length reduce or increment of DNA are regarded as the most effective routes of studying the binding mode of compounds to DNA in the absence of crystallographic NMR and structural data. For further explaining of the binding mode, viscosity measurements were made. Under appropriate conditions, a traditional intercalative mode such as intercalation of standard material like ethidium bromide leads to a significant increment in the viscosity of DNA solution due to an increment in the

Table 7
Spectral parameters for the interaction of the prepared imine complexes.

Complex	λ_{max} free (nm)	λ_{max} bound (nm)	Δn	Chromism (%)[a]	Type of chromism	Binding constant 10^4 (K_b)[b]	ΔG* kJ mol^{-1}
HNPNMn	452	463	11	21.8	Hypo	2.12	− 24.68
	477	493	16	31.1	Hypo		
	377	378	1	31	Hypo		
HNPNNi	478	468	10	64.4	Hypo	5.58	− 27.08
	386	400	14	75.96	Hypo		
HNPNV	422	440	18	27.68	Hyper	3.74	− 26.09
	347	354	7	21.6	Hyper		
HNPNCr	475	470	5	6.85	Hyper	9.17	− 28.31
	339	343	4	3.95	Hyper		
	396	391	5	4.4	Hyper		

[a] Chromism (%) = (Abs_{free} − Abs_{bound}) / Abs_{free}.
[b] Binding constant K_b = mol^{-1} dm^3.

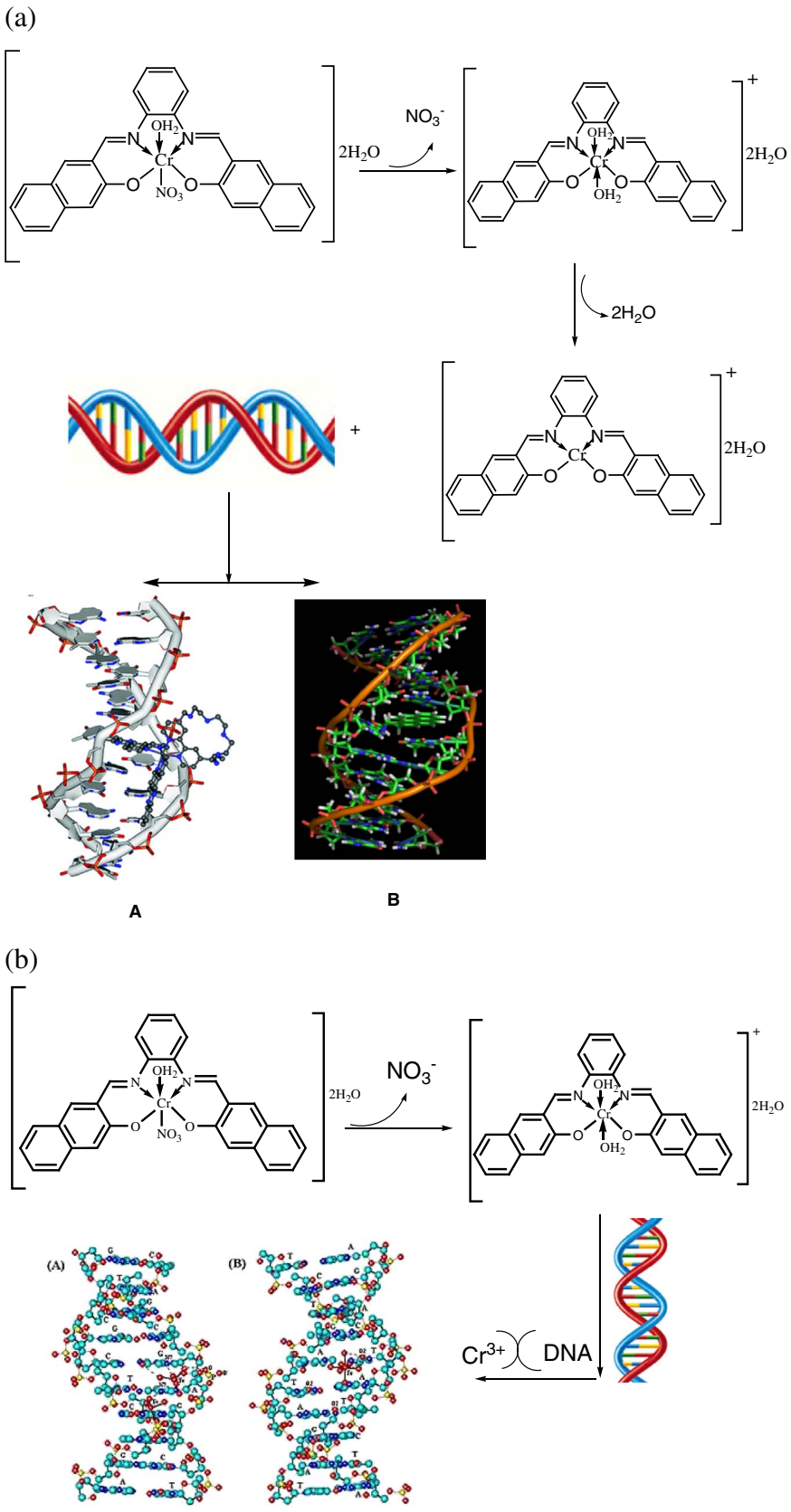

Scheme 3. (a): Suggested mechanism for interaction of HNPNCr with DNA via (A) intercalation binding and (B) replacement.(b): Suggested mechanism for interaction of HNPNCr with DNA via groove binding (electrostatic and hydrogen bond).

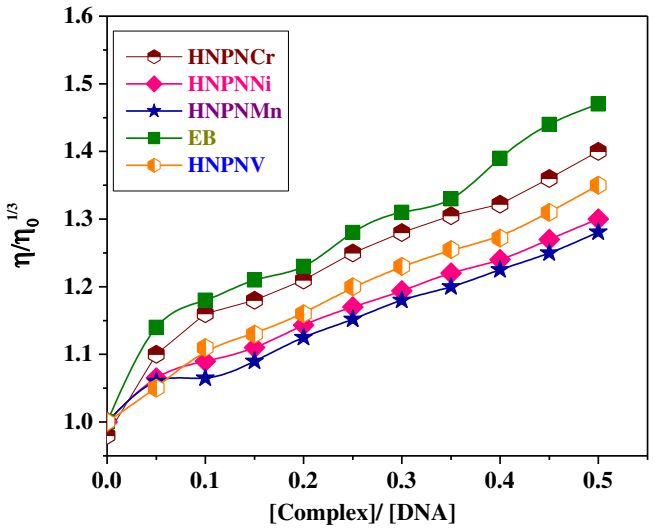

Fig. 7. The effect of increasing concentration of the prepared HNPNCr, HNPNNi, HNPNMn and HNPN V complexes compared to standard ethidium bromide (EB) on the relative viscosities of DNA at [DNA] = 0.5 mM, [complex] and [EB] = 25–250 μM and 298 K.

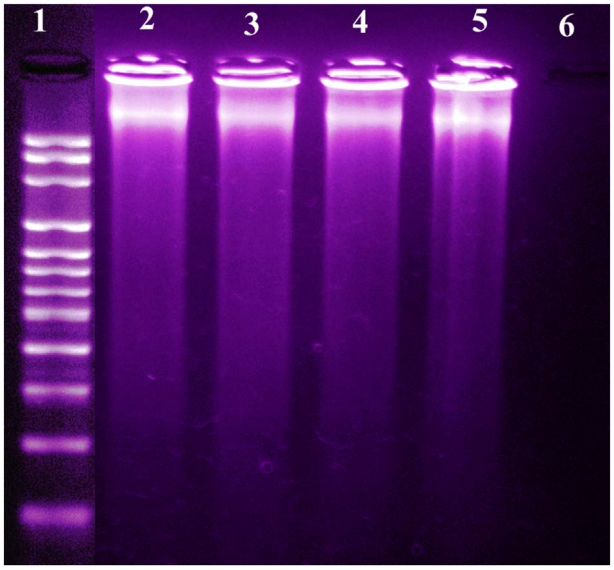

Fig. 8. DNA binding results of the prepared imine complexes based on gel electrophoresis. Lane 1: DNA Ladder, lane 2: HNPNCr + DNA; lane 3: HNPNV + DNA; lane 4: HNPNMn + DNA, lane 5: HNPNNi + DNA, lane 6: HNPNNi.

segregation of base pairs at the intercalation site and thus an increment in the overall DNA length. On other hand, drug molecules attachment exclusively to the DNA grooves lead to less pronounced in DNA solution viscosity [5,11,12,41] a partial intercalation of compound may bend the DNA helix, resulting in the reduction of its effective length and, concomitantly, its viscosity [5,11–15,42,43]. The relative viscosity of DNA solution enhances significantly as the concentration of the compound raises, as shown in Fig. 7. This may be due to the admission of the aromatic ring in imine ligand into the DNA base pairs leading to a crook in the DNA helix, hence, increase in the segregation of the base pairs at the intercalation place and increment in DNA molecular length. Moreover, the sequence of the observed increment in the viscosity values was renovated with the binding affinity to DNA i.e. HNPNCr complex shows the highest binding affinity to DNA and the highest viscosity. Moreover, HNPNCr complex could be bind to DNA via electrostatic binding as shown in Scheme 3(b). Electrostatic binding may appear due water molecules replace coordinated nitrate group. Thus, HNPNCr complex will be charged (cf. Scheme 3b) and electrostatic interaction occurs between the positive charge in the complex and base pair of DNA.

3.3.3. Gel Electrophoresis

Agarose gel electrophoresis is used for the DNA binding studies. The prepared imine chelates were studied for their DNA binding activity by agarose gel electrophoresis method (cf. Fig. 8). The gel after electrophoresis clearly showed that the intensity of all the treated DNA samples has partially detracted, possibly because of the interaction with DNA. The partial binding of DNA was observed in the prepared imine chelates. The difference was clarified in the bands of the complexes compared to that of the control DNA. This explains that the control DNA alone does not show any significant cleavage whereas the complexes show cleavage [22,34,44]. However, the nature of reactive intermediates involved in the DNA binding by the complexes is not obvious. These results show that the metal ions play an important role in the interaction with isolated DNA. As the compound was observed to bind with DNA, it can be concluded that the compound inhibits the growth of the pathogenic organism by interaction with genome. The studies reveal that partial binding of DNA was observed by VO(II), Mn(II), Cr (III) and Ni(II) imine complexes. The experimental results suggested that the checked complexes could bind to DNA via intercalative mode.

3.4. Anticancer Activity

Study of cancer is one of the most famous research topic of many scientists and researchers in the world. There are so many cells in the human body. When these cells, as a part of the body, begin to grow out of domination then cancer starts. After Cardiovascular disease, cancer is a disease which cause human death or which leads to human death. Now a days, there are so many drugs which are used for the treatment of cancer are cytotoxic. Modern cancer treatment is called chemotherapy.

Mechanism of anticancer activity includes,

i. Enzymatic or chemical inactivation:

Reactive carcinogens which represents not only on DNA but also acting on proteins or enzymes, can be inactivated directly. Different types of chemicals have a significant role in this inactivation. Anticancer characteristics occurred with both inhibitors and inducers of cytochrome P-450 enzymes.

ii. Prevention of formation of active species:

Many carcinogens or mutagens, which are genotoxic, needs metabolic activation or bio activation to an active species, which can combine with the DNA. This process is take place in the liver.

iii. Scavenging:

Many anticancer agents have the ability to sweep dietary carcinogens that occurs through adsorption or binding. In this process, carcinogens remains intact and are unable to combine with DNA.

iv. Antioxidant and free radical scavenging:

Free radicals play a considerable role in carcinogenesis. Because it has the ability to damage DNA and cause mutagenicity and cytotoxicity. Induction of mutations and inhibition of DNA repair approaches by the reactive oxygen species (ROS), results in the inactivation of some tumor suppressor genes, which leads to cancer. Medical plants provided anticancer agents which have good antioxidant or free radical scavenging property.

The cytotoxic potency of the prepared HNPN imine titled ligand and its complexes was evaluated against human Colon carcinoma cells (HCT-116 cell line), hepatic cellular carcinoma cells (HepG-2) and breast carcinoma cells (MCF-7 cell line within 0–10 μM concentration range. The IC_{50} values were evaluated for each compound and results are offered in Fig. 9 and Table S3. As shown, most complexes displayed manifestly cytotoxic potencies (which are greater than that of ligand) assisted to vinblastine standard drug. It seems that changing of the

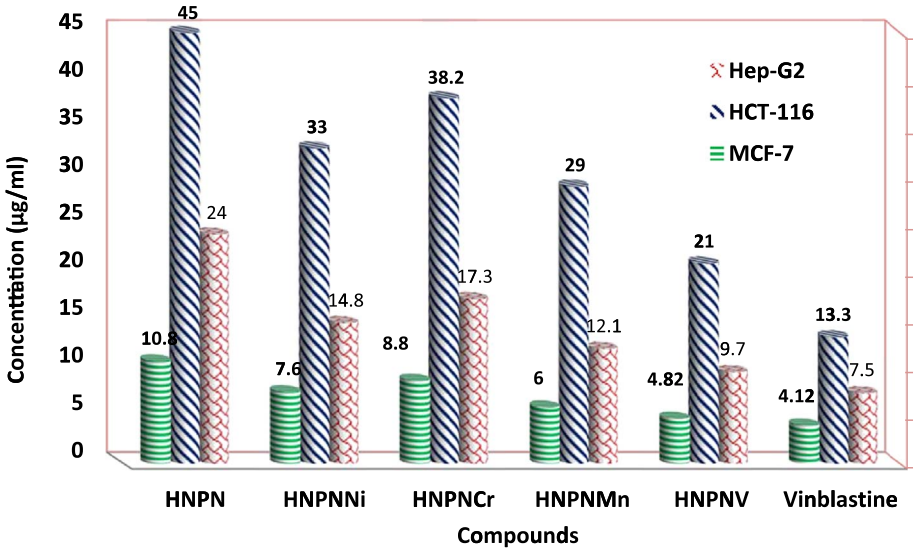

Fig. 9. IC_{50} values of the HNPN ligand and its complexes against human Colon carcinoma cells, (HCT-116 cell line) and colon carcinoma cells, (MCF-7 cell line).

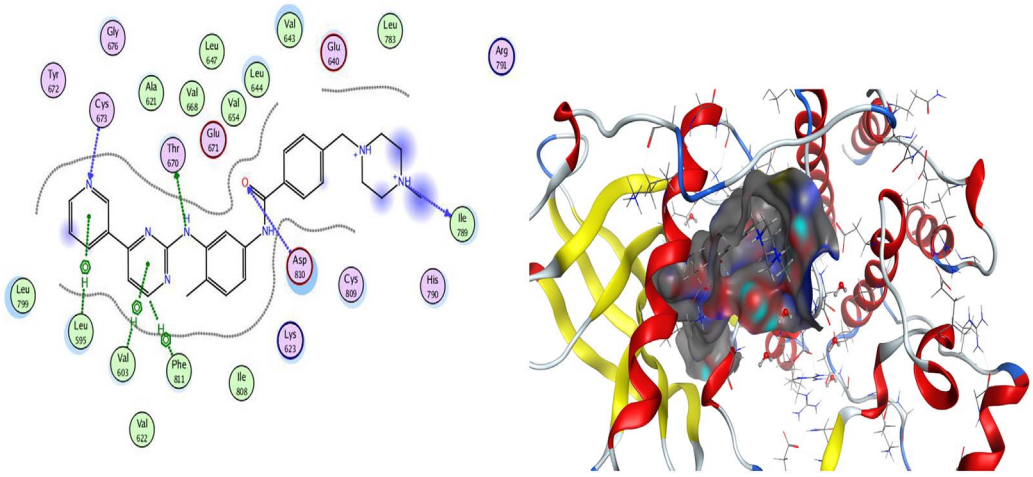

Fig. 10. The binding mode of the native ligand STI with C-kit exhibited one H-bond donor with THR 670 at distance 2.08 and one H-bond donor with ILE 789 at distance 2.19 and one H-bond donor with CYS 673 at distance 2.85 and one H-bond acceptor with HOH 1105 at distance 2.82 its score was -20.04 kcal mol^{-1}. (2D and 3D ligand-receptor interactions.)

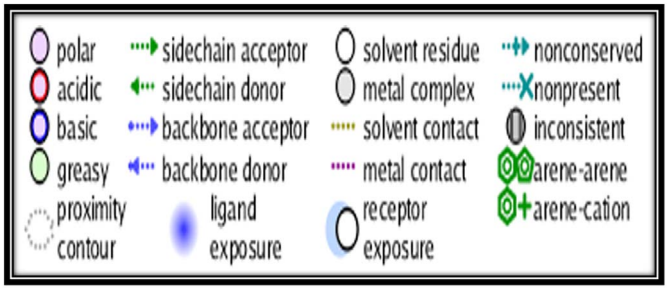

Scheme 4. Representative keys for the type of interactions between the substrate and THR 670.

complexation locations and the nature of the metal ion has impact on the biological way. Cytotoxicity potency of the investigated complexes could be rationalized to the focal metal atom which was presented by Tweedy's chelation theory [5,11,12,43–46]. Cytotoxicity conclusions indicated that all tested complexes (IC_{50} = 21–38.2 µg/µl) demonstrated potent cytotoxicity against HCT-116 cancer cells, (IC_{50} = 9.7–17.3 µg/µl) demonstrated potent cytotoxicity against HepG-2 cancer cells and (IC_{50} = 4.82–8.80 µg/µl) against MCF-7 cancer cells. The response of the investigated cancer cells towards the studied compounds follows the following order MCF-7 > HepG-2 > HCT-116 cancer cells. HNPNV complex showed the highest cytotoxicity effect with IC_{50} value of 4.82 µg/µl, followed by HNPNMn with IC_{50} value of 6.00 followed by HNPNNi complex with IC_{50} value 7.60 µg/µl and then HNPNCr complex with IC_{50} value 8.2 µg/µl in case of MCF-7 cancer cells. It was spotted also that all complexes are more potent than the free titled ligand. This indicated beneficent of the antitumor potency when coordination occurs. The refinement of cytotoxic potency may be specified to that the positive charge of the metal increased the acidity of coordinated titled ligand that gives protons, causing more potent hydrogen bonds which enhanced the biological activity [5,11,12,43]. It seems that changing the coordination locations and the nature of the metal ion has a significant effect on the biological manner by modifying the binding ability of DNA [12,14,15,43,47]. Gaetke and Chow had reported that metal has been suggested to smooth oxidative tissue damage through a free-radical mediated trajectory analogous to the Fenton reaction [5,12,48].

3.5. Molecular Modeling

3.5.1. Molecular Modeling: Docking Study

The prepared compounds were analyzed for the binding affinity of tyrosine kinases receptor (PDB 1t46) for the purpose of both investigate the interaction between studied compounds and c-kit receptor and for

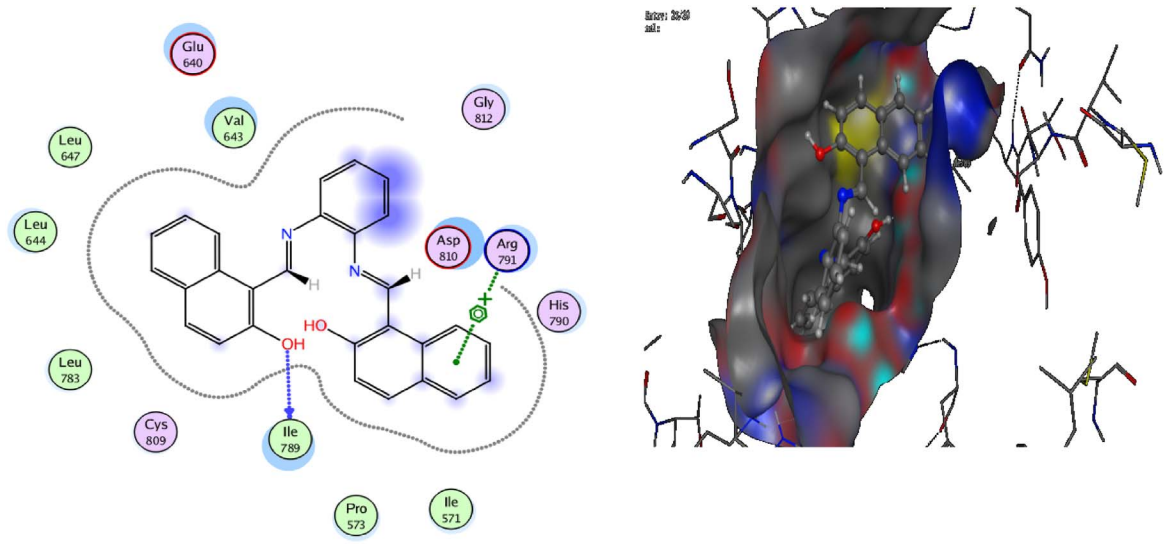

Fig. 11. The proposed binding mode of HNPN ligand docked in the active site of TRK protein; (2D and 3D ligand-receptor interactions). The binding mode of the ligand with C-kit receptor exhibited one H-bond acceptor with Ile789 1105 at distance 1.89; and one hydrophobic interaction with Arg 791 at distance 3.13.

lead optimization. Molecular modeling calculation was carried out to investigate the binding free energies of these inhibitor inside the target c-kit kinase receptor.

3.5.2. Validation of the Docking Performance and Accuracy

Docking of the native co-crystallized STI-571 ligand (Imatinib or Gleevec) was used to establish the docking accuracy of the program. The docked HNPN imine ligand was exactly superimposed on the native co-crystallized one with RMSD being 0.40 A° and binding free energies of − 20.04 kcal·mol^{-1}. The hydrogen bonds between the docked HNPN imine ligand and the amino acids were the same as those between the amino acid and the native ligand.

3.5.3. The Binding Affinities of the Investigated Compounds Into c-kit Kinase Receptor

To compare affinity and to investigate the interaction between the investigated HNPN imine ligand and receptor, molecular docking study was done (cf. Fig. 10).

Scheme 4 illustrates the representative keys for the type of interaction between substrates and the THR 670, which can be used as a guide in the docking in Figs. 10, 11. For the docking calculation, firstly, the protein structure (PDB code: 1t46) was separated from the inhibitor and hydrogen atoms were added. The binding free energy, hydrogen bond and RMSD were used to evaluate the binding affinity [49]. All the investigated compounds were docked into the same binding site of the native co-crystallized ligand (cf. Figs. 11–15). Both HNPNV and HNPNNi complexes respectively, gave the best docking score − 16.14, − 15.21 (cf. Figs. 14, 15).

The binding energies of HNPN imine ligand HNPNCr, HNPNMn, HNPNNi, HNPNV, and (Imatinib or Gleevec) docked into the active site of TRK protein were − 14.56, − 14.47, − 16.14, − 15.21, − 13.89 and − 20.04 kcal/mol, respectively (cf. Figs. 10–15).

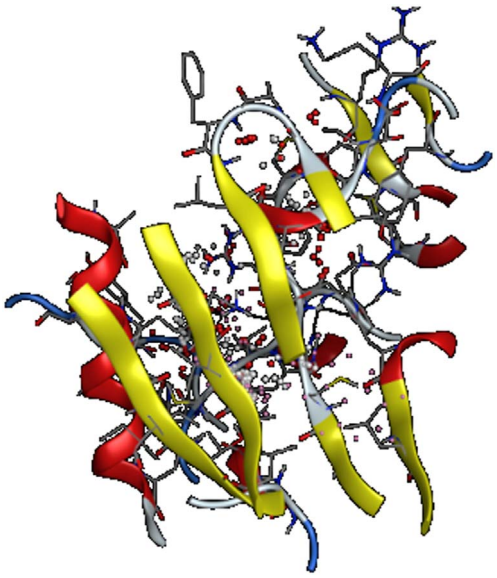

Fig. 12. The proposed binding mode of HNPNCr complex docked in the active site of TRK protein The binding mode of HNPNCr complex with C-kit receptor exhibited one H-bond acceptor with HOH 1105 at distance 2.64; and one H-bond acceptor with HOH 1105 at distance 2.63 and one H-bond acceptor with HOH 1106 at distance 3.32.

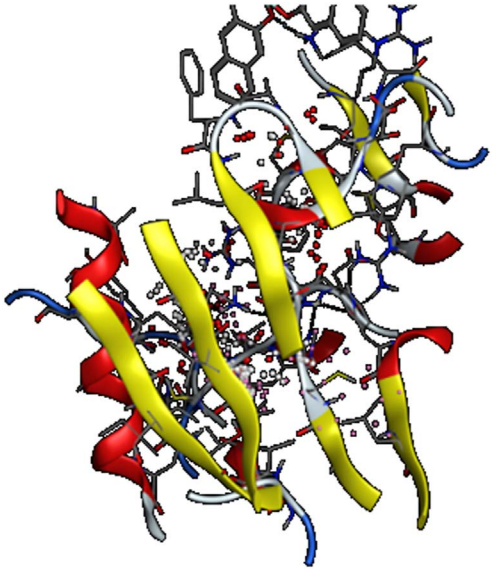

Fig. 13. The proposed binding mode of HNPNMn complex docked in the active site of TRK protein. The binding mode of HNPNMn complex with C-kit receptor exhibited one H-bond acceptor with HOH 1105 at distance 1.62; and one H-bond acceptor with HOH 1105 at distance 3.43.

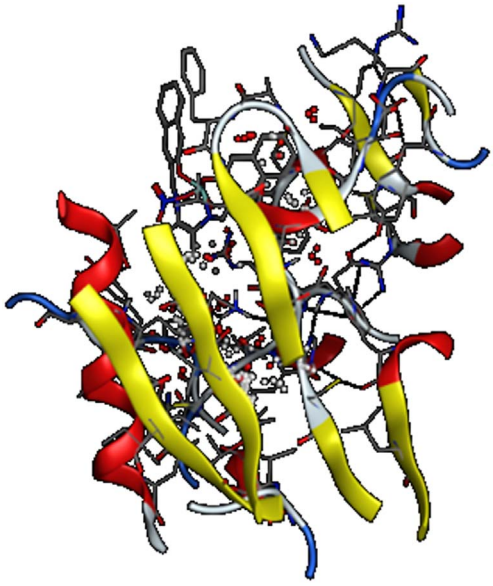

Fig. 15. The proposed binding mode of HNPNNi complex docked in the active site of TRK protein. The binding mode of HNPNNi complex with C-kit exhibited one H-bond acceptor with HOH 1033 at distance 3.16.

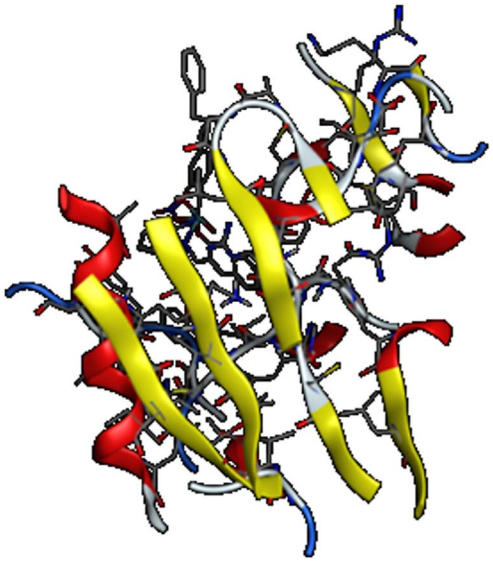

Fig. 14. The proposed binding mode of HNPNV complex docked in the active site The proposed binding mode of HNPNV complex docked in the active site of TRK protein of TRK protein. The binding mode of the Ni-complex with C-kit exhibited one H-bond acceptor with HOH 1033 at distance 2.56.

4. Conclusion

In this study three innovative VO(II), Cr(III), Mn (II), and Ni(II) imine complexes have been synthesized and their structures have been characterized by physicochemical and spectral tools. The obtained results demonstrated that the HNPN imine ligand behaves as dibasic tridentate ONO ligand and coordinates to VO(II), Cr(III) and Ni(II) in 1:1 molar ratio. From the analytical and spectral data, it is observed that the complexes adopted octahedral geometry in case of Cr(III) and Mn(II), square planner geometry in Ni(II) and square pyramidal geometry in VO(II). The anti-pathogenic screening showed that these complexes are perfect antimicrobial agents against different organisms and standards. Moreover, the interaction of the complexes with CT-DNA has been effectively examined and explored by electronic absorption, viscosity measurements and gel electrophoresis. The DNA interaction studies propose the intercalative and replacement modes of interaction. Furthermore, the growth inhibitory effect of the prepared compounds was tested on HepG-2, HCT-116 and MCF-7cancer cells. Among these compounds, HNPNV complex significantly decreases the cell viability time and dose dependently. The synthesized compounds were investigated for the binding alliance of tyrosine kinases receptor (PDB1t46). MOE (molecular modeling environment) determined the binding free energies of these inhibitors into the target c-kit kinase receptor. It was found that.

the MOE were typically concise with the experimental data. These biological findings from our study would be helpful in perceptive of DNA interaction exposed by metal complexes and may progress to improve novel metal based therapeutic drugs.

Appendix A. Supplementary data

Supplementary data to this article can be found online at http://dx.doi.org/10.1016/j.jphotobiol.2017.04.003.

References

[1] N. Charef, F. Sebti, L. Arrar, M. Djarmouni, N. Boussoualim, A. Baghiani, S. Khennouf, A. Ourari, M.A. Al Damen, M.S. Mubarak, D.G. Peters, Polyhedron 85 (2015) 450.
[2] L.H. Abdel-Rahman, R.M. El-Khatib, L.A.E. Nassr, A.M. Abu-Dief, Russ. J. Gen. Chem. 83 (2013) 2510–2518.
[3] Ahmed M. Abu-Dief, Mohammed S.M. Abdelbaky, Santigo García-Granda, Acta Cryst E71 (2015) 496–497.
[4] Ahmed M. Abu-Dief, Ibrahim M.A. Mohamed, J. Basic Appl. Sci. 4 (2015) 119–133.
[5] L.H. Abdel-Rahman, A.M. Abu-Dief, R.M. El-Khatib, S.M. Abdel-Fatah, J. Photochem. Photobiol. B 162 (2016) 298–308.
[6] K.M. Khan, M. Khan, M. Ali, M. Taha, S. Rasheed, S. Perveen, M.I. Choudhary, Bioorg. Med. Chem. 17 (2009) 7795.
[7] K.C. Gupta, A.K. Sutar, Coord. Chem. Rev. 252 (2008) 1420–1450.
[8] K.C. Gupta, A.K. Sutar, C.C. Lin, Coord. Chem. Rev. 253 (2009) 1926–1946.
[9] K.C. Gupta, A.K. Sutar, J. Mol. Catal. A Chem. 272 (2007) 64–74.
[10] A.G.J. Ligtenbarg, R. Hage, B.L. Feringa, Coord. Chem. Rev. 237 (2003) 89–101.
[11] L.H. Abdel-Rahman, Rafat M. El-Khatib, Lobna A.E. Nassr, Ahmed M. Abu-Dief, Mohamed Ismael, A.S. Amin, Spectrochim. Acta 117 (2014) 366–378.
[12] Laila H. Abdel-Rahman, Ahmed M. Abu-Dief, Rafat M. El-Khatib, Shimaa Mahdy Abdel-Fatah, Bioorg. Chem. 69 (2016) 140–152.
[13] L.H. Abdel-Rahman, A.M. Abu-Dief, M. Ismael, M.A.A. Mohamed, N.A. Hashem, J. Mol. Struct. 1103 (2016) 232–244.
[14] L.H. Abdel-Rahman, A.M. Abu-Dief, E.F. Newair, S.K. Hamdan, J. Photochem. Photobiol. B 160 (2016) 18–31.
[15] Laila H. Abdel-Rahman, Nabawia M. Ismail, Mohamed Ismael, Ahmed M. Abu-Dief, Ebtehal Abdel-Hameed Ahmed, J. Mol. Struct. 1134 (2017) 851–862.
[16] W. Song, J. Cheng, D. Jiang, L. Guo, M. Cai, H. Yang, Q. Lin, Spectrochim. Acta A 121 (2014) 70.
[17] G. Li, K. Du, J. Wang, J. Liang, J. Kou, X. Hou, L. Ji, H. Chao, J. Inorg. Biochem. 119 (2013) 43.
[18] Laila H. Abdel-Rahman, Rafat M. El-Khatib, Lobna A.E. Nassr, Ahmed M. Abu-Dief, Russ. J. Gen. Chem. 84 (2014) 1830–1836.
[19] L.H. Abdel-Rahman, A.M. Abu-Dief, S.K. Hamdan, A.A. Seleem, Int. J. Nano. Chem. 1 (2015) 65–77.
[20] L.H. Abdel-Rahman, A.M. Abu-Dief, M.S.S. Adam, S.K. Hamdan, Catal. Lett. 146 (2016) 1373–1396.
[21] L.H. Abdel Rahman, A.M. Abu-Dief, N.A. Hashem, A.A. Seleem, Int. J. Nano. Chem. 1 (2015) 79–95.
[22] Laila H. Abdel-Rahman, Ahmed M. Abu-Dief, H. Mostafa, Samar Kamel Hamdan, Appl. Organomet. Chem. 31 (2017) e3555.
[23] A.M. Abu-Dief, L.A.E. Nassr, J. Iran. Chem. Soc. 12 (2015) 943–955.
[24] M.I. Hossain, M. Switalska, W. Peng, M. Takashima, N. Wang, M. Kaiser, J. Wietrzyk, S. Dan, T. Yamori, T. Inokuchi, Eur. J. Med. Chem. 69 (2013) 294–309.
[25] A.M. Abu-Dief, I.F. Nassar, W.H. Elsayed, Appl. Organomet. Chem. 30 (2016) 917–923.
[26] Molecular Operating Environment (MOE), Chemical Computing Group, Inc., Montreal, Quebec, Canada, 2008.
[27] C.D. Mol, D.R. Dougan, T.R. Schneider, R.J. Skene, M.L. Kraus, D.N. Scheibe, et al., Structural basis for the autoinhibition and STI-571 inhibition of C-Kit tyrosine kinase, J. Biol. Chem. 279 (2004) 31655–31663.
[28] A.N.M.A. Alaghaz, M.E. Zayed, S.A. Alharbi, R.A.A. Ammar, J. Mol. Struct. 1087 (2015) 60–67.
[29] Laila H. Abdel-Rahman, R.M. El-Khatib, Ahmed M. Abu-Dief, S.M. Abdel-Fatah, A.A. Sleem, Int. J. Nano.Chem. 2 (2016) 83–89.
[30] A.M. Abu-Dief, R. Díaz-Torres, E.C. Sañudo, L.H. Abdel-Rahman, N.A. Alcalde, Polyhedron 64 (2013) 203–208.
[31] A.A.A. Emara, Spectrochm Acta A 77 (2010) 117–125.
[32] L.H. Abdel-Rahman, R.M. El-Khatib, L.A.E. Nassr, A.M. Abu-Dief, F.E.D. Lashin, Spectrochim. Acta Part A 111 (2013) 266–276.
[33] S. Sarkar, K. Dey, S. Biswas, B.B. Bhaumik, J. Coor. Chemi. 11 (2007)

1143–1156 (60).
[34] A.E. Ouf, M.S. Ali, E.M. Saad, S.I. Mostafa, J. Mol. Struct. 973 (2010) 69–75.
[35] M. Shakir, M.A. Sherwani, O. Mohammad, M. Azam, S. Al-Resayes, J. Photochem. Photobiol. B 157 (2016) 39–56.
[36] T.A. Yousef, G.M. Abu El-Reash, I.M. Gabr, O.A. El-Gammal, R.A. Bedier, J. Mol. Struct. 1029 (2012) 149–160.
[37] Hany M. Abd El-Lateef, Ahmed M. Abu-Dief, A.A. Moniur, J. Mol. Struct. 1130 (2017) 522–542.
[38] Hany M. Abd El-Lateef, Ahmed M. Abu-Dief, Bahaa El-Dien M. El-Gendy, J. Electroanal. Chem. 758 (2015) 135–147.
[39] Hany M. Abd El-Lateef, Ahmed M. Abu-Dief, L.H. Abdel-Rahman, Eva Carolina Sañudo, Núria Aliaga-Alcalde, J. Electroanal. Chem. 743 (2015) 120–133.
[40] Laila H. Abdel-Rahman, Rafat M. El-Khatib, Lobna A.E. Nassr, Ahmed M. Abu-Dief, Inter. J. Chem. Kin. 46 (2014) 543–553.
[41] D.S. Raja, S.P. Bhuvanesh, K. Natarajan, Jo. Biolog. Inorg. Chem. 17 (2012) 223–237.
[42] L.H. Abdel-Rahman, A.M. Abu-Dief, N.M. Ismail, M. Ismael, Inorg. and Nano-Metal Chem. 47 (2017) 467–480.
[43] L.H. Abdel-Rahman, A.M. Abu-Dief, M. Basha, Azza A. Hassan Abdel-Mawgoud, Appl. Organomet. Chem. (2017) e3750, , http://dx.doi.org/10.1002/aoc.3750.
[44] Y. Liu, W. Mei, J. Lu, H. Zhao, L. He, F. Wu, J. Coord. Chem. 61 (2008) 3213–3224.
[45] G. Yang, F.Z. Wu, L. Wang, L. NianFi, X. Tina, J. Inorg. Biochem. 66 (1997) 141–144.
[46] B. Tweedy, Phytopathology 55 (1964) 910–914.
[47] G. Feng, J.C. Mareque-Rivas, N.H. Williams, Chem. Commun. 17 (2006) 1845–1847.
[48] L.M. Gaetke, C.K. Chow, Toxicology 189 (2003) 147–163.
[49] Sami A. Al-Harbi, Mahmoud S. Bashandy, Hammed M. Al-Saidi, Adel A.A. Emara, Tarek A.A. Mousa, Spectrochim. Acta A Mol. Biomol. Spectrosc. 145 (2015) 425–439.